Carboxymethyl guar gum nanoparticles for drug delivery applications: preparation and preliminary *in-vitro* investigations

G. Dodi[1,2*], A. Pala[3], E. Barbu[4], D. Peptanariu[5], D. Hritcu[1], M. I. Popa[1], , B.I. Tamba[6]

[1] "Gheorghe Asachi" Technical University of Iasi, Romania

[2] SCIENT - Research Centre for Instrumental Analysis, Bucharest, Romania

[3] University of Sassari, Sassari, Italy

[4] University of Portsmouth, Portsmouth, UK

[5] "Petru Poni" Institute of Macromolecular Chemistry, Iasi, Romania

[6] "Gr. T. Popa" University of Medicine and Pharmacy, Iasi, Romania

* Tel: +40 232 278683, Fax: +40 232271311, E-mail address: gianina.dodi@yahoo.co.uk

Abstract

Carboxymethyl guar gum (CMGG) synthesised from commercially available polysaccharide was formulated into nanoparticles *via* ionic gelation using trisodium trimetaphosphate (STMP) as cross-linking agent. Characterisation using a range of analytical techniques (FTIR, NMR, GPC, TGA and DLS) confirmed the CMGG structure and revealed the effect of the CMGG and STMP concentration on the main characteristics of the obtained nanoformulations. The average nanoparticle diameter was found to be around 208 nm, as determined by dynamic light scattering (DLS) and confirmed by scanning electron microscopy (SEM) and nanoparticle tracking analysis (NTA). Experiments using simulated gastric and intestinal fluids evidenced significant pH-dependent drug release behaviour of the nanoformulations loaded with Rhodamine B (RhB) as a model drug (loading capacity in excess of 83%), as monitored by UV-Vis. While dose-dependent cytotoxicity was observed, the nanoformulations appeared completely non-toxic at concentrations below 0.3 mg/mL. Results obtained so far suggest that carboxymethylated guar gum nanoparticles formulated with STMP warrant further investigations as polysaccharide based biocompatible drug nanocarriers.

Keywords: carboxymethyl guar gum, phosphate, nanoparticles, cytotoxicity, drug delivery.

1. Introduction

Guar gum (GG) is a non-ionic natural polysaccharide sourced from the seeds of C*yamopsis tetragonolobus* (*Leguminosae* family) and consists of linear chains of (1, 4)-β-D-mannopyranosyl units with α-D-galactopyranosyl units attached *via* (1, 6) linkages (Figure 1). Because of its ability to produce highly viscous aqueous solutions at lower concentrations, guar gum is used in many applications in industries such as, textile, petroleum, paper, food, explosives and pharmaceuticals (Patel et al., 2014) - it is biocompatible, biodegradable, non-toxic, low-cost and amenable to chemical

modifications, properties that make it an ideal material for developing drug delivery formulations (Prabaharan, 2011). However, native guar gum has also shortcomings such as, uncontrolled rates of hydration, high swelling, thickening effect, instability upon storage, high susceptibility to microbial attack and the difficulty to control viscosity due to relative fast biodegradation (Yadav et al., 2008). Various strategies were developed in order to overcome these issues, offering the opportunity to tailor the physical and chemical properties of guar gum thus yielding materials that may find a wide range of applications. Many approaches dependent on chemical modification of guar gum were aimed at meeting the requirements of special applications (Rana et al., 2011) and included derivatisation reactions such as methylation (Risica et al., 2005), sulfation (Wang et al., 2013), hydroxyalkylation (He at al., 2008; Kono et al., 2015), carboxymethylation (Dodi et al., 2011; Gong et al., 2012), or phosphorylation (Niu et al., 2013). Carboxymethylation in particular has been found to improve water solubility while increasing the solution viscosity, to lower biodegradability and hence increase the shelf life compared to that of the native polysaccharide (Narasimha et al., 2004).

Carboxymethyl guar gum was formulated as microparticles tailored for drug delivery applications (Parveen et al., 2012) and the studies indicated that these drug microcarriers were able to avoid rapid clearance by phagocytes and thus had an extended circulation into the blood stream (Balan & Verestiuc, 2014; Kumari et al., 2010). Microencapsulation of sensitive macromolecules such as, proteins into derivatized carboxymethyl guar gum was also achieved by using multivalent metal ions solutions (Ca^{2+} and Ba^{2+}) as cross-linkers (Thimma & Tammishetti, 2001). The maximum retention of bovine serum albumin (BSA) in the beads was only about 50% under the studied conditions, which could be due to the lower rates of cross-linking. Microspheres of carboxymethyl guar gum loaded with abacavir sulfate were formulated using water-in-oil (w/o) emulsions and glutaraldehyde (GA) as cross-linker; it was found that the beads extended the *in vitro* release time in both acidic and alkaline pH conditions when compared with unmodified GG (Sullad et al., 2011). Carboxymethyl guar gum was also combined with gelatine to obtain semi-interpenetrating polymer networks (semi-IPN) in the form of microspheres that were prepared by emulsion cross-linking method using GA and loaded with theophylline (an antasthmatic drug) (Phadke et al., 2014); the results suggested a potential toxicity of the microspheres due to the presence of GA and demonstrated an encapsulation efficiency ranging from 56 to 74 %, which was found to be affected by the amounts of CMGG and cross-linking agent. Congo Red, a hydrophobic dye commonly used for diagnosis and potentially useful as a therapeutic agent, was encapsulated recently into alginate-carboxymethyl guar gum hydrogel microspheres prepared by the extrusion of the biopolymer mixture in the presence of calcium chloride (Bosio et al., 2014). The

hydrogel microsphere structure was considered to play a key role in the controlled release of the model drug. Spherical carboxymethyl guar gum nanoparticles in the size range of 12–30 nm were successfully prepared *via* nanoprecipitation and sonication methods (Gupta & Verma, 2014); it was found that the stability of CMGG nanoparticle suspensions was dependent on the nature of the solvent and on the sonication time, parameters that can be optimized further to tailor CMGG nanoformulations for a wide range of applications. Although nanoprecipitation and sonication are eco-friendly and cost-effective methods to produce nanosized carboxymethyl guar gum nanoparticles, the main disadvantage is the poor stability, property necessary to get a proper drug delivery system with optimal control release. However, the nanoparticles need to be stabilized against dissolution at different pH by cross-linking, a process in which the free functional groups are partially consumed ( ). Cross-linking of carboxymethyl guar gum functional groups may also reduce the high swelling characteristics of this material and provide better control of drug release from various dosage forms such as microspheres, particles or beads. STMP is a non-toxic cyclic triphosphate often used for the preparation of cross-linked hydrogels and microspheres for pharmaceutical applications (Dulong et al., 2004; Gliko-Kabir et al., 2000; Mocanu et al., 2004). However, to the best of our knowledge, the preparation of carboxymethylated guar gum nanoparticles by ionic gelation with STMP has not been reported in the literature.

The aim of this work was to investigate the possibility to formulate cost-effectively carboxymethyl guar gum nanoparticles for biomedical applications such as drug delivery using trisodium trimetaphosphate (STMP) as cross-linker.

2. Experimental

2.1. Materials

Guar gum (Mw 220 kDa), trisodium trimetaphosphate $Na_3P_3O_9$ (STMP), Rhodamine B (RhB) and sodium hydroxide (NaOH) were purchased from Sigma-Aldrich, Germany. Chloroacetic acid (CAA) was obtained from Merck, Germany. Ethanol and acetone were procured from the Chemical Company (Iasi, Romania). Analytical grade chemicals were used as received without further purification. All solutions were prepared with ultrapure water (18.2 MΩ•cm).

2.2. Guar gum purification

Commercial guar gum was purified as described in the literature (Cunha et al., 2007) with some modifications. Briefly, commercial guar gum (5 g) was extracted with ethanol (Soxhlet, 72 h) and hydrated in ultrapure water (500 mL) under magnetic stirring (3 h); after centrifugation (1500 rpm; 605 RCF; 15 min), the supernatant was precipitated in acetone and the solid was filtered and washed successively with ethanol and ultrapure water, and subsequently freeze-dried (batch denoted GG).

2.3. Preparation of carboxymethyl guar gum

The synthesis of carboxymethyl guar gum was performed as previously reported (Dodi et al., 2011) with slight modifications. Briefly, 1 g of GG was dispersed in 100 mL of ultrapure water and the mixture was stirred for 2 h under nitrogen atmosphere. The resulting suspension was mixed with 20 mL of NaOH solution (0.1 M) and the mixture was allowed to react for 2 h at room temperature (25°C). Chloroacetic acid (20 mL; 1.58 g/cm^3; 0.025 mol) was added and the mixture was stirred overnight at 50° C. The reaction mixture was then cooled to ambient temperature, adjusted to pH 7.0 (using 1 M HCl), extracted with acetone and separated by centrifugation (5 000 rpm; 6142 RCF; 10 min). The product was further purified by dialysis against distilled water until neutral pH has been reached (approx. 72 h). The final product (batch denoted CMGG) was then dried by lyophilisation and stored in a desiccator for further analysis.

2.4. Preparation of cross-linked nanoparticles

Varying amounts of CMGG (concentration ranging from 0.05 to 0.2 % w/v) were added into a 2M NaOH aqueous solution (100 mL; pH=12.0) and were allowed to hydrate for a minimum of 2 h under constant magnetic stirring at room temperature. A STMP aqueous solution (100 mL; concentration varying from 0.2 to 10%, w/v, as described in Table 1) was then added at a flow rate of 1 mL/min using a peristaltic pump, and the reaction mixture was then continuously stirred overnight. The resultant colloidal dispersion was dialyzed against distilled water until neutral pH (approx. 72 h). An aliquot of the sample suspension was kept for particle size measurements, while the remaining product was lyophilized by freeze drying and then stored in a desiccator. Preliminary experiments informed the preparation of 11 formulations, details of which are given in Table 1.

2.5. Characterization

2.5.1. NMR spectroscopy

The ^{1}H and ^{13}C-NMR spectra were recorded on a Jeol NMR 400 MHz spectrometer at 70 °C in D_2O using sodium trimethlysilyl propionate (TSP) as internal reference.

2.5.2. FTIR-ATR spectroscopy

The FTIR spectra were recorded on dried samples using a Nexus FT-IR Diamond HTR instrument (Thermo Scientific) in the range of 400–4000 cm^{-1} using a Smart Orbit ATR accessory with diamond crystal and were processed using Omnic 8.0 software.

2.5.3. Gel permeation chromatography (GPC)

The average molecular mass (M_w) and the polydispersity index (PDI) of the guar gum derivatives were determined by gel permeation chromatography (GPC) on a Polymer Laboratories

System (PL-GPC 120, Varian) instrument equipped with refractive index detector and three PL-aquagel-OH packed columns (8 µm particle size and 20, 40 and 60Å pore type), connected in series. Chromatographic parameters were as follows: eluent (0.2M $NaNO_3$; 0.01M NaH_2PO_4; pH=7) flow rate 1 mL/min; column temperature 30°C; sample volume 100 µL. Pullulan standards (Type P-82, Lot 01101, Shodex Denko KK, Japan) with sample weights of 0.6×10^4, 1×10^4, 2.17×10^4, 4.88×10^4 and 11.3×10^4, 21×10^4, 36.6×10^4, 80.5×10^4 g/mol were used as standards.

Samples were prepared by dissolving 0.1 ±0.001g of polymer in 10 mL eluent stirred at room temperature overnight, with the subsequent filtration of the solution through a syringe filter with a pore diameter of 0.45 µm. All data were recorded and processed using Cirrus GPC software.

2.5.4. Thermal analysis (TG-DTG)

Thermogravimetric analysis was carried out on a Mettler Toledo TGA-SDTA851 system, in nitrogen atmosphere with a flow rate of 50 mL/min, at a heating rate of 10 K/min in the temperature range of 25–700 °C; sample weight range 4–5 mg.

2.5.5. Surface morphology

The surface morphology of nanoparticles was investigated by scanning electron microscopy using a SEM Jeol JSM-6060LV instrument. Samples were deposited on stubs, dried with nitrogen and coated with golden alloy in an argon atmosphere (current 20 mA, pressure 10^{e-3} Pa) using a coater (Quorum, Q 150RES).

2.5.6. Particle size and zeta potential measurements

The average hydrodynamic diameter of the nanoparticles was determined in water at 25 °C by dynamic light scattering measurements using a Malvern Zetasizer ZS90 (Malvern Instruments, Worcester, UK). The same instrument allowed the determination of zeta potential ξ (mean of three measurements) and polydispersity index (PDI).

In addition, real-time dynamic nanoparticle visualization was performed by nanoparticle tracking analysis (NTA) using a NanoSight LM10 instrument equipped with a sample chamber with a 532 nm laser and a 560 nm long pass filter. The particle size was calculated using the Stokes–Einstein equation.

2.6. *In vitro* experiments

Cell cultures

For cytotoxicity tests, normal human dermal fibroblasts (NHDF) cells (from PromoCell) at a passage number lower than 10 were grown in T25 culture flasks with 10 mL of DMEM:F12 medium (from Lonza) supplemented with 10% fetal bovine serum (FBS, Gibco), 1 mM sodium pyruvate

(Lonza) and 1 % Penicillin-Streptomycin-Amphotericin B mixture (10K/10K/25 µg in 100 mL, Lonza). Cell growing was done at 37 °C and 5 % CO_2 under humidified atmosphere and medium was changed with fresh one every 4 days. NHDF cells were harvested by trypsinization with Trypsin-Versene (EDTA) mixture (Lonza), washed with phosphate buffered saline (PBS, Invitrogen) centrifuged at 200 rpm for 5 min, counted and seeded at a density of $5x10^3$ cells/well in 96 well plates with 100 µL/well of the above specified medium. Cells were incubated and were allowed to adhere in humidified atmosphere at 37°C until the next day.

Cytotoxicity assay (MTS)

The cytotoxicity induced by CMGG nanoparticles (batch Np11) was investigated by CellTiter 96®AQueousOne Solution Cell Proliferation Assay (MTS) (Promega Corporation, Madison, Wisconsin, USA). The metabolic cell activity (an indirect measure of cytotoxicity) was measured by quantifying the conversion of MTS to formazan, which can be photometrically detected. The quantity of the formazan product as measured at 490 nm is directly proportional to the number of living cells in a culture. The cells were exposed for 24 and 48 h to different concentrations of nanoparticles (batch Np11) ranging from 0.78 to 100 mg/mL, in 100 µL fresh medium. The plates were incubated at 37 °C and 5 % CO2 under humidified atmosphere for 24 or 48 h. Four hours before reading the results, 20 µL of CellTiter 96®AQueousOne Solution reagent were pipetted into each well and the plates were returned to the incubator. The absorbance was then recorded with an EnVision Multilabel Plate Reader (PerkinElmer). A total of eight serial dilutions were tested and the experiment was repeated three times.

Data analysis was done with GraphPad Prism version 6.04 for Windows (GraphPad Software, San Diego, CA). To calculate the half maximal inhibitory concentrations (IC50), a log (inhibitor) vs. response with variable slope (four parameters) nonlinear regression model was used. At least 3 replicates were included in the analysis.

Optical microscopy

NHDF cells were seeded at a density of $35x10^3$ cells/well in six well plates with 2 mL/well of medium. Cells were allowed to attach in humidified atmosphere at 37°C until the next day. The medium was replaced with serial dilutions of nanoparticles (batch Np11, dispersed in 2 mL fresh medium) and the cells were incubated at 37 °C and 5 % CO_2 under humidified atmosphere for the next 24 or 48 h. Images were recorded using an inverted microscope Leica DMI 3000 under modulation contrast (MC) at the beginning of experiment, and then 24 and 48 h after incubation with nanoparticles.

2.7. RhB loading and release studies

To determine the actual amount of the entrapped model drug, 100 mg of CMGG nanoparticles (batch Np11 was chosen based on its size distribution) were added in a water-ethanol (1:1) solution of RhB (20 mL; 2 % w) and stirred for 3 h at room temperature. The mixture was adjusted to pH 5.0 using HCl (0.01M) and was left overnight under stirring. The supernatant was separated by centrifugation (13.400 rpm; 12.927 RCF; 20 min) and measured by UV–Vis using a Perkin Elmer Lambda 35 spectrophotometer at 554 nm. The drug entrapment efficiency (E_e) was calculated from a calibration curve of RhB using the following equation (Vasi et al., 2014):

$$E_e(\%) = \frac{M_i - M_f}{M_i} \times 100, \quad (1)$$

where M_i is the initial weight of the RhB added and M_f is the amount of free RhB in the supernatant. The RhB-loaded nanoparticles were washed with ultrapure water in order to remove the unreacted components and then freeze-dried.

The release studies of RhB (Np11_RhB) were carried out as follows: dehydrated RhB loaded nanoparticles (10 mg) were suspended at 37 °C in 5 mL phosphate buffer solutions (0.1 M; pH 2.2 and 7.4, respectively) in an incubated thermostatic shaker (100 rpm). At periodic intervals, a 150 μL aliquot was withdrawn and measured by UV–Vis in a 10 mm micro-cell. The amount of the released drug was calculated using a calibration curve.

3. Results and discussion

3.1. CMGG synthesis and characterisation

Following purification of commercial guar gum by removal of insoluble fractions as well as sugar and protein contaminants, carboxymethylation of the purified guar gum was carried out *via* a consecutive two-step reaction as previously reported in the literature (Dodi et al., 2011), with minor modifications (Figure 1). The carboxymethylated guar gum obtained following reaction optimisation (labelled CMGG) had a degree of substitution of 0.62 %.

Figure 1

The formation of CMGG was confirmed by ^{1}H and ^{13}C-NMR results (Figure 2), which were in good agreement, with other studies (Manna et al., 2015). The ^{1}H-NMR spectrum showed new proton peaks at 3.77, 3.95 and 4.22 ppm, attributed to the methylene protons from the carboxyl group, in addition to the anomeric (4.70 and 5.03 ppm) and sugar protons (3.57 and 4.13 ppm) found in the raw GG. ^{13}C-NMR spectra of CMGG confirmed the presence of a carbonyl peak at 180 ppm, while the carbon peaks of mannose and galactose appeared in the range 90–110 ppm and the rest of the side chain in the range 60–80 ppm. Successful carboxymethylation was confirmed in the FTIR spectra of

CMGG (Figure 3) by the presence of additional peaks (1732, 1413 and 1230 cm^{-1}) corresponding to the COO^- symmetric and asymmetric stretching vibrations; moreover, a shift of the OH stretching band (3354 cm^{-1}) in the GG spectrum to 3333 cm^{-1} in CMGG, and an increase of the band intensity (both rationalized by an increase in hydrogen bonding interaction consequent to the introduction of a carboxylic group and) were observed.

Figure 2

GPC measurements indicated a higher molecular weight (M_w) for CMGG compared to GG (Table 1), as a direct result of the introduction of carboxymethyl groups onto the polysaccharide backbone. The carboxymethylation step increased considerably the solubility of the modified galactomannan chains compared to GG and also led to an improved polydispersity index.

Table 1

3.2. Determination of the nanoparticles optimum reaction conditions

The synthesized carboxymethyl guar gum was successfully formulated into nanoparticles by using STMP as an ionic gelation agent (Figure 1). Cross-linking was achieved through the formation of phosphoester linkages between the CMGG chains, in two steps: the opening of the STMP ring by CMGG in the presence of sodium hydroxide was followed by the reaction with another polymer chain and the release of sodium pyrophosphate. The reaction between the carboxylated polysaccharidic chains and STMP under basic conditions resulted overall in nanoparticulate, three-dimensional hydrogel networks.

To optimize the conditions for cross-linking in an attempt to yield stable nanoformulations with uniform size distribution, a series of CMGG particles (batches 1–11) were prepared from CMGG by varying the concentration of CMCG and SMTP, as presented in Table 2. The cross-linker/polysaccharide ratios were calculated according to the assumption that each mole of STMP reacts with three pairs of hydroxy groups (Gliko-Kabir et al., 2000).

It was found that a larger particle size was obtained as the concentration of both polymer (CMGG) and cross-linker (SMTP) increased. When the concentration of both components was low (e.g. CMGG -0.05% and STMP 5%), the mean diameter of the nanoparticles was about 208.8 ± 0.87 nm; this could perhaps be attributed to a lower number of macromolecules being linked together as part of the same particle and to better packing (due to stronger inter and intra molecular interactions allowed by the higher flexibility of the lightly cross-linked polymer chains). The PDI values indicate a broad size distribution (Table 2). The negative ζ-potential measured for all nanoparticles (expected due to the presence of CMGG terminal carboxylic groups in combination with phosphate groups) contribute to

the particle good stability (without any aggregation) observed during storage at room temperature. According to Akasov et al. (2015) the high negative surface charge of the polysaccharide formulations is a key factor to stabilize colloidal dispersions. Following the optimisation step, the batch labelled Np11 (Table 2) was selected for further investigations.

Table 2

FTIR measurements of the CMGG nanoparticles (batch Np11) showed the appearance of a shoulder of low intensity at 1225 cm^{-1} that corresponds to P=O stretching (Shalviri et al., 2010), and a shoulder of increased intensity at 1090 cm^{-1} that was attributed to P–O–C deformation vibrations (Braz et al., 2007). The increased intensity in the 874-1225 cm^{-1} region is considered therefore a clear indication of the presence of phosphate groups in the prepared nanoparticles.

Figure 3

Figure 4 presents the thermogram (1st derivative) of STMP cross-linked nanoparticles overlayed with those of the guar gum and carboxymethylated guar gum. The results of the thermogravimetric analysis indicate the presence of stronger hydrogen bonding following carboxymethylation of the guar gum, possibly due to an increase in free water content (from 8.54 % in GG to 10.69 % in CMGG, Table 3). The thermal stability of CMGG (reflected in the temperature of the peak in the first derivative spectra, corresponding to the main degradation step) appears slightly lower (241 ºC; 57 % mass loss) than for GG (262 ºC; 70 % mass loss), while a second degradation step appears at considerable higher temperatures (478 ºC; 9.56 % mass loss) due to the carboxymethyl groups that make possible increased inter- and intra-molecular interactions that ultimately impart higher thermal stability (Tripathy et al., 2008). It was interesting however to observe that the nanoparticles (CMGG cross-linked with SMTP) had the major mass loss step at a much higher decomposition temperature than the native guar and CMGG, likely due to the fact that the cross-linking reaction increases the average molecular mass and the intermolecular interactions, which in turn increase considerably the thermal stability of the nanoparticles.

Figure 4

Table 3

To complement the results of DLS analysis, NTA studies investigated in more detail the particle size distribution of samples in liquid suspension (Figure 5A). The average particle size results were in good agreement with both DLS and SEM data.

Figure 5

The results of SEM analysis confirmed the almost spherical surface morphology of the synthesized CMGG nanoparticles ((Figure 6A). When in dry state, nanoparticles tend to self-assemble into secondary clusters with grape-like morphology, as a result of the Van der Waals and other inter-particle forces closely correlated with the very high surface area to volume ratio.

Figure 6

3.3. *In-vitro investigations*

The results of dose-response cytotoxicity tests carried out on NHDF cells using MTS after 24 h incubation with CMGG nanoparticles demonstrated no significant toxic effect at concentrations up to 0.3 mg/mL (Figure 7). Cell viability was found to decrease substantially with an increase in nanoparticle concentration up to 25 mg/mL, with a calculated IC50 value of 4.715 mg/mL.

Figure 7

While not application-specific, NHDF cell lines represent a suitable and convenient model for preliminary cytotoxicity assessment. The growth behaviour of the cells in the presence of CMGG nanoparticles was monitored using optical microscopy, using NHDF cell adhesion as an indicator of viability since the cells detach during apoptosis (furthermore, cell spread can also give an indication of the nature of interactions with nanoparticles present in the media, as an adherent cell which has increased its spreading area is considered to show active proliferation (Rosman et al., 2014). NHDF cell proliferation, distribution and adhesion of the cells following incubation with CMGG nanoparticles were examined at different time points (24 h and 48 h, respectively) and different nanoparticle concentration (1.56 mg/mL and 3.125 mg/mL), Figure 8. Even after 48 h, the NHDF cells incubated with nanoparticles at a concentration of 1.56 mg/mL show a good distribution and cover almost the entire substrate, suggesting reasonably good compatibility with the nanoparticles. However, cell proliferation appears to start being affected after 48 h in contact with nanoparticles at concentration reaching 3 mg/mL.

We attribute the excellent biocompatibility of the samples to the sugars of the polymer backbone, sugars which are suitable for the cell growing. Also, the higher cell compatibility of CMGG nanoparticles could be related to surface charge (Akasov et al., 2015), explained by their ability to interact with the positively charged fibroblast surface. These data indicates that surface modification can be modulated in order to design drug delivery systems with more predictable clinical outcomes.

Figure 8

3.4. RhB entrapment efficiency and drug release studies

The lack of toxicity at low concentrations (0.3 mg/mL or less) makes CMGG nanoparticles a good candidate to be considered for drug delivery applications. A hydrophilic fluorescent marker, RhB was chosen as model drug for its lack of toxicity at easily detectable concentrations, strong absorption and emission spectra, and good stability to pH variations (Figure 1). RhB was successfully entrapped into nanoparticles with high efficiency (E_e of 83.2 %, for batch Np11_RhB). To optimize the effect of drug concentration on the entrapment efficiency, different concentrations of RhB were tested in the range of 0.25 to 5 mg/mL (Table 4). It was found that high RhB concentrations led to low entrapment efficiency (ranging overall between 33.5 % and 83.2 %), with an optimum found at 0.5 mg/mL RhB.

Table 4

A substantial change in size distribution, zeta potential and polydispersity index was observed for the drug loaded nanoparticles compared to the unloaded ones. As expected, the drug loaded nanoparticles had a larger mean diameter and lower negative ζ-potential (in absolute values) following the entrapment of RhB, with the colloidal stability not being noticeably affected. The RhB loaded nanoparticles were also analysed using NTA in fluorescence mode (Figure 5B); while noticeable photo bleaching limited the sensitivity of the measurement, the results confirmed the presence of RhB within the nanoparticles and an increase in the mean diameter compared to unloaded nanoparticles, and were consistent with the of DLS results.

SEM investigations confirmed as well the size increase following loading with RhB, with images showing discrete and near spherical (slightly elongated) nanoparticles, well separated from one another (Figure 4B) and with low polydispersity (confirming again DLS results, where PDI measured was 0.08).

Drug release behaviour was investigated in simulated gastric (pH 2.2) and intestinal (pH 7.4) fluids at 37 ^{0}C as suggested in the literature (Li & Liu, 2008; Chaurasia et al. (2006) and Subrahmanyam (2012)). Figure 9 presents the release profiles for the Np11_RhB batch. A burst release of 13% was observed for both pH values just after the addition of loaded nanoparticles, likely due to a fraction of RhB present on the surface of the nanoparticles being immediately released in contact with the simulated fluids. The RhB released in acidic medium over the total duration of the experiment reached only 37.1 % while in alkaline conditions the model drug was released almost completely (92.7 %), indicating that the release of RhB from the CMGG nanoparticles can be controlled by pH.

Figure 9

To investigate the mechanism of the RhB release, the initial release data was fitted in the Ritger and Peppas equation (Popa et al., 2010; Ritger & Peppas, 1987):

$$\frac{M_t}{M_\infty} = kt^n, \quad (2)$$

where M_t/M_∞ is the mass ratio of the drug released from nanoparticles at time point t compared to equilibrium; k is a characteristic constant related to the structure of the polymeric network; and n is a diffusion exponent. Constants k and n were calculated from the slopes and intercepts of the graph $\ln M_t/M_\infty \; vs \ln t$. The k and n constants are related to a specific transport mechanisms, which normally consider the relative rates of drug diffusion, matrix swelling and polymeric network relaxation. Three main models are typically employed to describe the behaviour of the swelling polymeric network that releases the drug in aqueous solutions: Fickian diffusion (n = 0.5); non-Fickian, anomalous diffusion ($0.5<n<1$); and zero order release (n = 1.0) (Mullarney et al., 2006). The values obtained at (n = 0.5) suggests an anomalous diffusion mechanism close to the Fickian model for acidic conditions (pH 2.2) and a non-Fickian diffusion release process (n = 0.83) in an alkaline environment (pH 7.4).

4. Conclusions

Guar gum - a biocompatible, biodegradable, low cost, accessible and versatile polysaccharide of natural origin can be easily converted into carboxymethyl guar gum, which was successfully formulated into nanoparticles by ionic cross-linking complexation with a non-toxic and inexpensive cross-linking agent, trisodium trimetaphosphate. The reaction conditions were optimized through careful investigation of the effects of polymer and cross-linker concentration upon particle size distribution, ζ-potential and polydispersity. Following optimization, DLS results revealed a relatively uniform size distribution of CMGG nanoparticles around 208 nm, also confirmed by NTA and SEM analysis. Cytotoxicity studies using NHDF cell cultures and MTS assays demonstrated that CMGG nanoparticles are non-toxic at concentrations below 300 µg/mL. To investigate the potential of CMGG nanoparticles for drug delivery applications, RhB was employed as a model drug and it was found that the drug initial concentration significantly influenced the entrapment efficiency, which ranged from 33.5 % to 83.2 %. Release studies at 37 ºC in simulated gastric and intestinal fluids indicated a slow and prolonged release of RhB from CMGG nanoparticles over several hours, and demonstrated that the release process can be controlled by pH. Overall, the results presented demonstrate the potential of nanoparticles formulated from CMGG *via* ionic gelation with trisodium trimetaphosphate for the development of sustained and controlled drug delivery systems.

Acknowledgements

The work was financially supported by The Romanian National Authority for Scientific Research, CNCS – UEFISCDI, project number PN-II-ID-PCCE-2011-2-0028.

References

Akasov, R., Borodina, T., Zaytseva, E., Sumina, A., Bukreeva, T., Burov, S., Markvicheva, E., 2015. Ultrasonically Assisted Polysaccharide Microcontainers for Delivery of Lipophilic Antitumor Drugs: Preparation and in Vitro Evaluation, Applied Materials & Interfaces 7, 16581−16589.

Balan, V., Verestiuc, L., 2014. Strategies to improve chitosan hemocompatibility: A review, European Polymer Journal 53, 171–188.

Bosio, V.E., Basu, S., Abdullha, F., Villalba Chacon, M.E., Guida, J.A., Mukherjee, A., Castro, G.R., 2014. Encapsulation of Congo Red in carboxymethyl guar gum–alginate gel microspheres, Reactive & Functional Polymers 82, 103–110.

Braz, R., Hechenleitner, A.A., Cavalcanti, O.A., 2007. Extraction, structural modification and characterization of Lotus Roots polysaccharides (*Nelumbo nucifera* Gaertn) excipient with potential application in modified drug delivery systems, Latin American Journal of Pharmacy 26, 706-10.

Chaurasia, M., Chourasia, M.K., Jain, N.K., Jain, A., Soni, V., Gupta, Y., Jain, S.K., 2006. Cross-Linked Guar Gum Microspheres: a viable approach for improved delivery of anticancer drugs for the treatment of colorectal cancer, Journal of American Association of Pharmaceutical Science Technology 7, 143-151.

Cunha, P.L., Paula, R.C., Feitosa, J.P., 2007. Purification of guar gum for biological applications, International Journal of Biological Macromolecules 41, 324–331.

Dodi, G., Hritcu, D., Popa, M.I., 2011. Carboxymethylation of guar gum: synthesis and characterization, Cellulose Chemistry and Technology 45, 171-176.

Dulong, V., Lack, S., Le Cerf, D., Picton, L., Vannier, J.P., Muller, G., 2004. Hyaluronan-based hydrogels particles prepared by crosslinking with trisodium trimetaphosphate. Synthesis and characterization, Carbohydrate Polymers 57, 1–6.

Gliko-Kabir, I., Yagen, B., Penhasi, A., Rubinstein, A., 2000. Phosphated crosslinked guar for colon-specific drug delivery: I. Preparation and physicochemical characterization, Journal of Controlled Release 63, 121–127.

Gong, H., Liu, M., Chen, J., Han, F., Gao, C., Zhang, B., 2012. Synthesis and characterization of carboxymethyl guar gum and rheological properties of its solutions, Carbohydrate Polymers 88, 1015–1022.

Gupta, A.P., Verma, D.K., 2014, Preparation and characterization of carboxymethyl guar gum nanoparticles, International Journal of Biological Macromolecules 68, 247–250.

He, L.S., Jiang, B., Wang, K., 2008. Determination of the degree of the substitution of hydroxyethyl guar gum, Carbohydrate Polymers 72, 557–560.

Kono, H., Hara, H., Hashimoto, H., Shimizu, Y., 2015. Nonionic gelation agents prepared from hydroxypropyl guar gum, Carbohydrate Polymers 117, 636–643.

Kumari, A., Yadav, S.K., Yadav, S.C., 2010. Biodegradable polymeric nanoparticles based drug delivery systems, Colloids and Surfaces B: Biointerfaces 75, 1-18.

Li, S., Liu, X., 2008. Synthesis, characterization and evaluation of semi-IPN hydrogels consisted of poly (methacrylic acid) and guar gum for colon-specific drug delivery, Polymer Advanced Technology 19, 371–376.

Manna, P.J., Mitra, T., Pramanik, N., Kavitha, V., Gnanamani, A., Kundu, P.P., 2015. Potential use of curcumin loaded carboxymethylated guar gum grafted gelatin film for biomedical applications, International Journal of Biological Macromolecules 75, 437-446.

Mocanu, G., Mihai, D., Le Cerf, D., Picton, L., Muller, G., 2004. Synthesis of new associative gel microspheres from carboxymethyl pullulan and their interactions with lysozyme, European Polymer Journal 40, 283–289.

Mullarney, M.P., Seery, T.A., Weiss, R.A., 2006. Drug diffusion in hydrophobically modified N,N-dimethylacrylamide hydrogels, Polymer 47, 3845–3855.

Narasimha, M.S., Hiremath, S.R., Paranjothy, K.L., 2004. Evaluation of carboxymethyl guar films for the formulation of transdermal therapeutic systems, International Journal of Pharmaceutics 272, 11–18.

Niu, S., Wang, J., Zhao, B., Zhao, M., Nie, M., Wang, X., Yao, J., Zhang, J., 2013. Regioselective synthesis and antioxidant activities of phosphorylated guar gum, International Journal of Biological Macromolecules 62, 741– 747.

Parveen, S., Ranjita, M., Sahoo, S.K., 2012. Nanoparticles: A Boon to Drug Delivery, Therapeutics, Diagnostics and Imaging, Nanomedicine: Nanotechnology, Biology and Medicine 8, 147-166.

Patel, J.J., Karve, M., Pate, N.K., 2014. Guar gum: a versatile material for pharmaceutical industries, International Journal of Pharmacy and Pharmaceutical Sciences 6, 13-19.

Phadke, K.V., Manjeshwar, L.S., Aminabhavi, T.M., 2014. Biodegradable polymeric microspheres of gelatin and carboxymethyl guar gum for controlled release of theophylline, Polymer Bulletin 71, 1625–1643.

Popa, N., Novac, O., Profire, L., Lupusoru, C.E., Popa, M.I., 2010. Hydrogels based on chitosan–xanthan for controlled release of theophylline, Journal of Materials Science: Materials in Medicine 21, 1241–1248.

Prabaharan, M., 2011. Prospective of guar gum and its derivatives as controlled drug delivery systems: Review, International Journal of Biological Macromolecules 49, 117–124.

Rana, V., Rai, P., Tiwary, A.K., Singh, R.S., Kennedy, J.F., 2011. Modified Gums: Approaches and applications in drug delivery, Carbohydrate Polymers 83, 1031-1047.

Ritger, P.L., Peppas, N.A., 1987. A simple equation for description of solute release I. Fickian and non-fickian release from non-swellable devices in the form of slabs, spheres, cylinders or discs, Journal of Controlled Release 5, 23-36.

Risica, D., Dentini, M., Crescenzi, V., 2005. Guar gum methyl ethers. Part I. Synthesis and macromolecular characterization, Polymer 46, 12247–12255.

Rosman, C., Pierrat, S., Tarantola, M., Schneider, D., Sunnick, E., Janshoff, A., Sönnichsen, C., 2014. Mammalian cell growth on gold nanoparticle-decorated substrates is influenced by the nanoparticle coating, Beilstein Journal of Nanotechnology 5, 2479–2488.

Shalviri, A., Liu, Q., Abdekhodaie, M.J., Wu, X.Y., 2010. Novel modified starch–xanthan gum hydrogels for controlled drug delivery: Synthesis and characterization, Carbohydrate Polymers 79, 898–907.

Subrahmanyam, P.J., 2012. Design and development of guar gum and borax cross-linked guar gum matrix tablets of theophylline for colon specific drug, Journal of Chemical Pharmaceutical Research 4, 1052-1060.

Sullad, A.G., Manjeshwar, L.S., Aminabhavi, T.M., 2011. Microspheres of Carboxymethyl Guar Gum for In Vitro Release of Abacavir Sulfate: Preparation and Characterization, Journal of Applied Polymer Science 122, 452–460.

Thimma, R.T., Tammishetti, S., 2001. Barium chloride crosslinked carboxymethyl guar gum beads for gastrointestinal drug delivery, Journal of Applied Polymer Science 82, 3084–3090.

Tripathy, J., Mishra, D.K., Srivastava, A., Mishra, M.M., Behari, K., 2008. Synthesis of partially carboxymethylated guar gum-g-4-vinyl pyridine and study of its water swelling, metal ion sorption and flocculation behavior, Carbohydrate Polymers 72, 462–472.

Vasi, A.M., Popa, M.I., Tanase, E.C., Butnaru, M., Verestiuc, L., 2014. Poly(acrylic acid)–poly(ethylene glycol) nanoparticles designed for ophthalmic drug delivery, Journal of Pharmaceutical Sciences 103, 676–686.

Wang, J., Niu, S., Zhao, B., Wang, X., Yao, J., Zhang, J., Zhao, W., Zhao, Y., 2013. Regioselective synthesis of sulfated guar gum: Comparative studies of structure and antioxidant activities, International Journal of Biological Macromolecules 62, 734– 740.

Yadav, M., Mishra, D.K., Behari K., 2011. Synthesis of partially hydrolyzed graft copolymer (H-partially carboxymethylated guar gum-g-methacrylic acid): A superabsorbing material, Carbohydrate Polymers 85, 29-36.

Figure captions

Figure 1. Schematic diagram for carboxymethylation, CMGG nanoparticles formulation and RhB loading

Figure 2. ^{1}H and ^{13}C-NMR spectra of GG and CMGG

Figure 3. FTIR-ATR spectra of native GG, CMGG sample and CMGG nanoparticles

Figure 4. TG curves (1^{st} derivative) of native GG, CMGG sample and CMGG nanoparticles

Figure 5. NTA images of typical tracks of particles moving under Brownian and a smoothed 3D plot of size distribution *vs.* particle concentration for A. CMGG nanoparticles (batch NP11) and B. loaded particles analysed under fluorescent (optically filtered) mode *vs.* particle concentration (batch Np11_RhB)

Figure 6. Morphology of A. CMGG nanoparticles (batch Np11) and B. loaded nanoparticles (batch Np11_RhB)

Figure 7. Cellular viability MTS assay on NHDF cells of CMGG nanoparticles

Figure 8. NHDF cell distribution, adhesion and morphology following incubation of CMGG nanoparticles using optical microscopy images

Figure 9. RhB release profiles in simulated gastric and intestinal fluids

Figure

Click here to download high resolution image

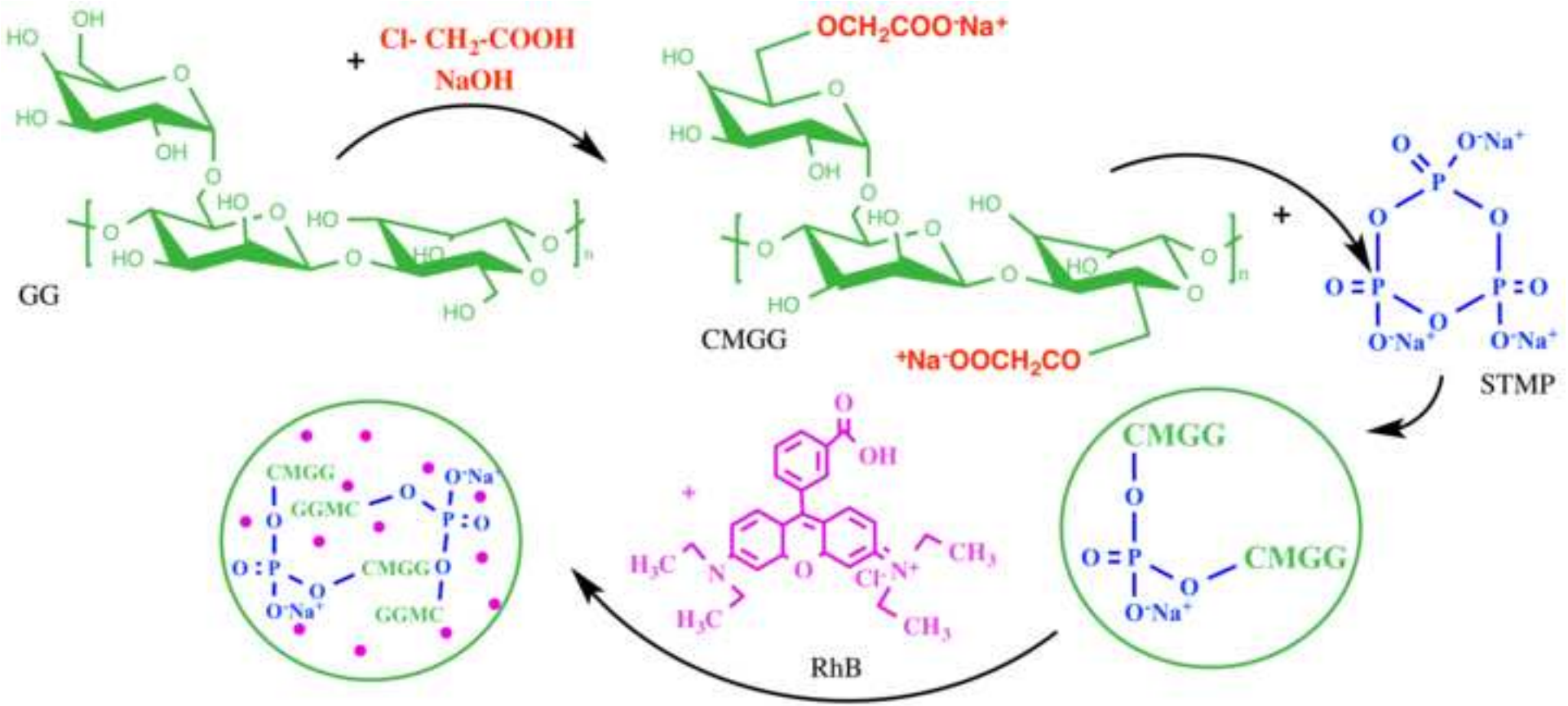

Figure

Click here to download high resolution image

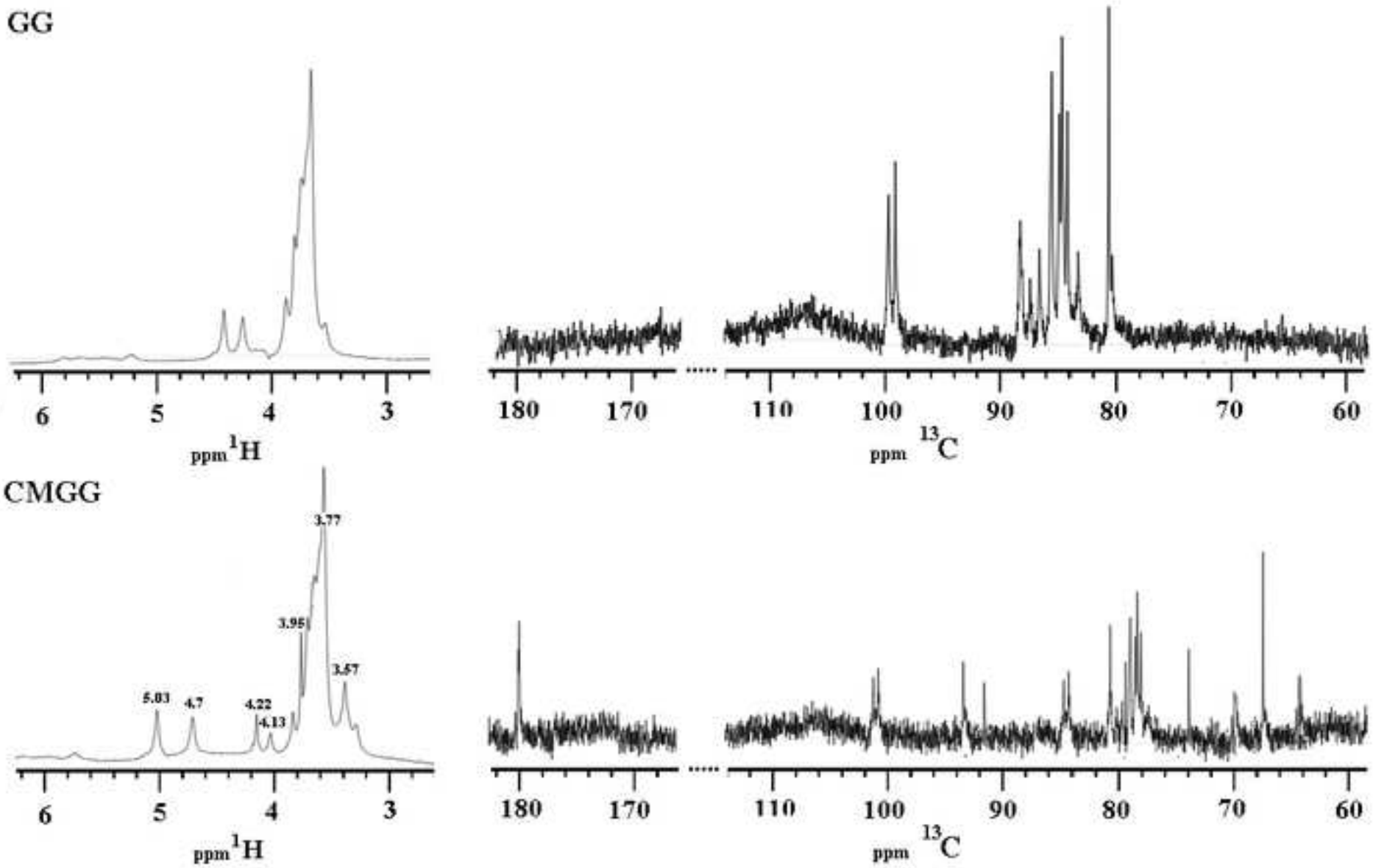

Figure

Click here to download high resolution image

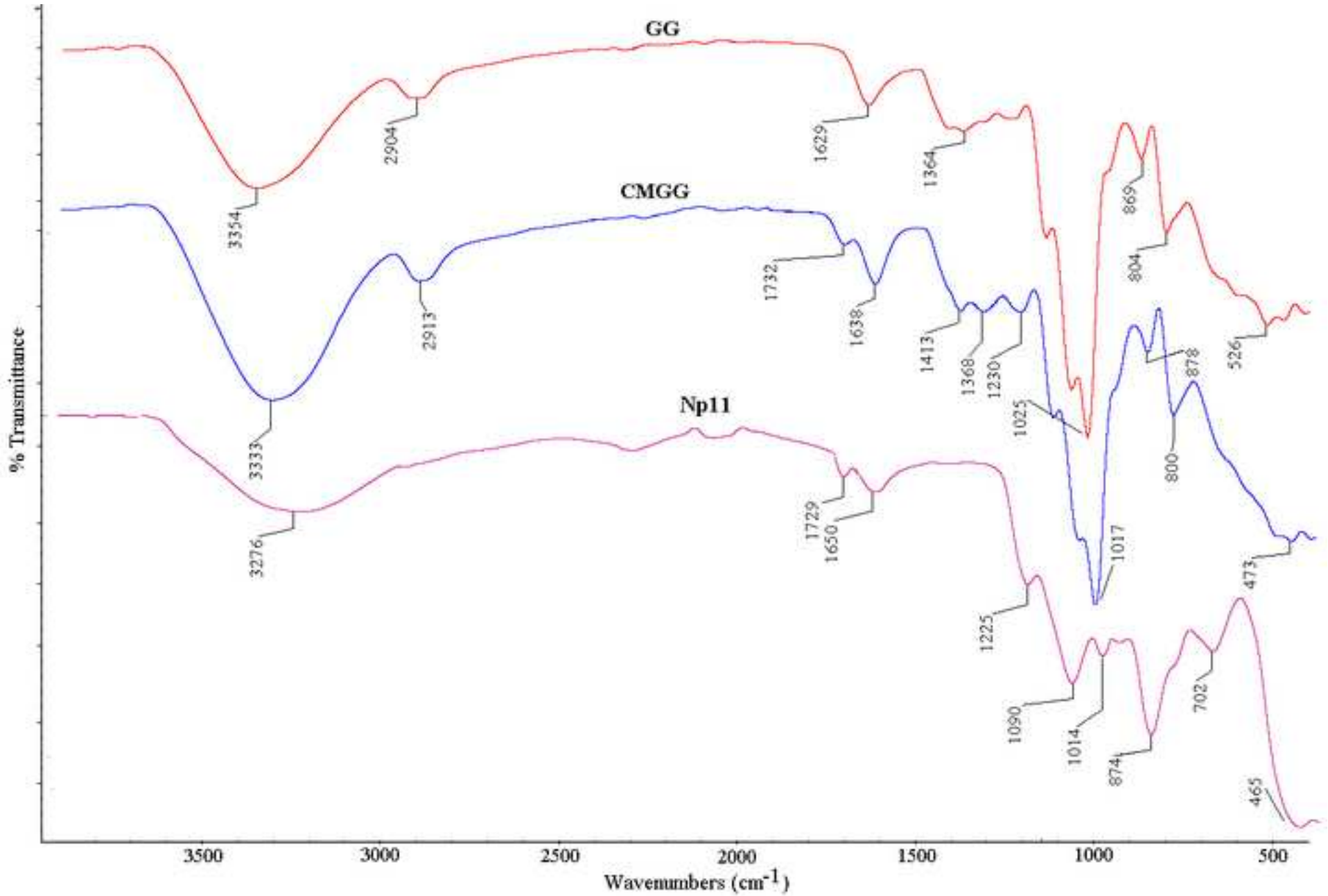

Figure

Click here to download high resolution image

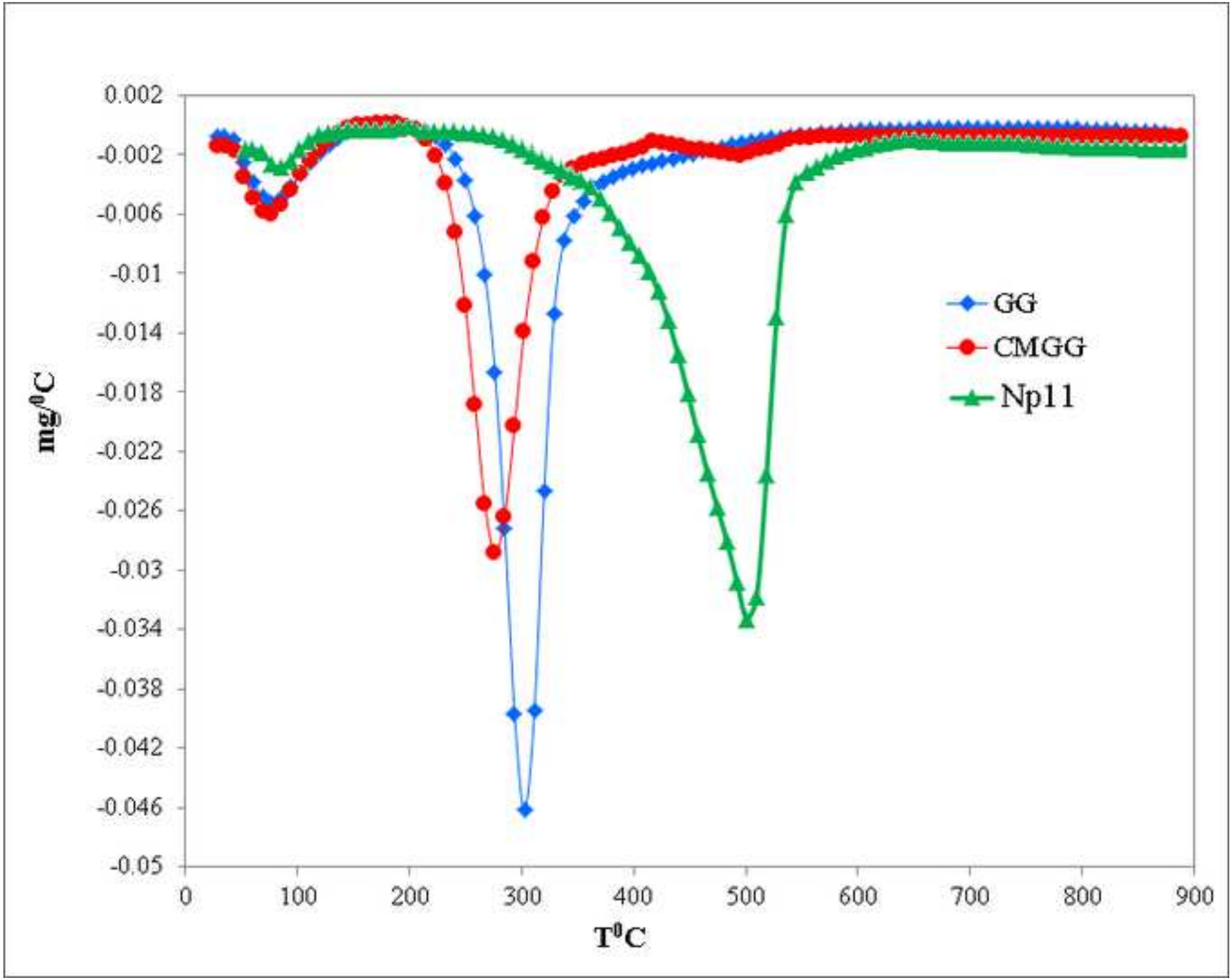

Figure

Click here to download high resolution image

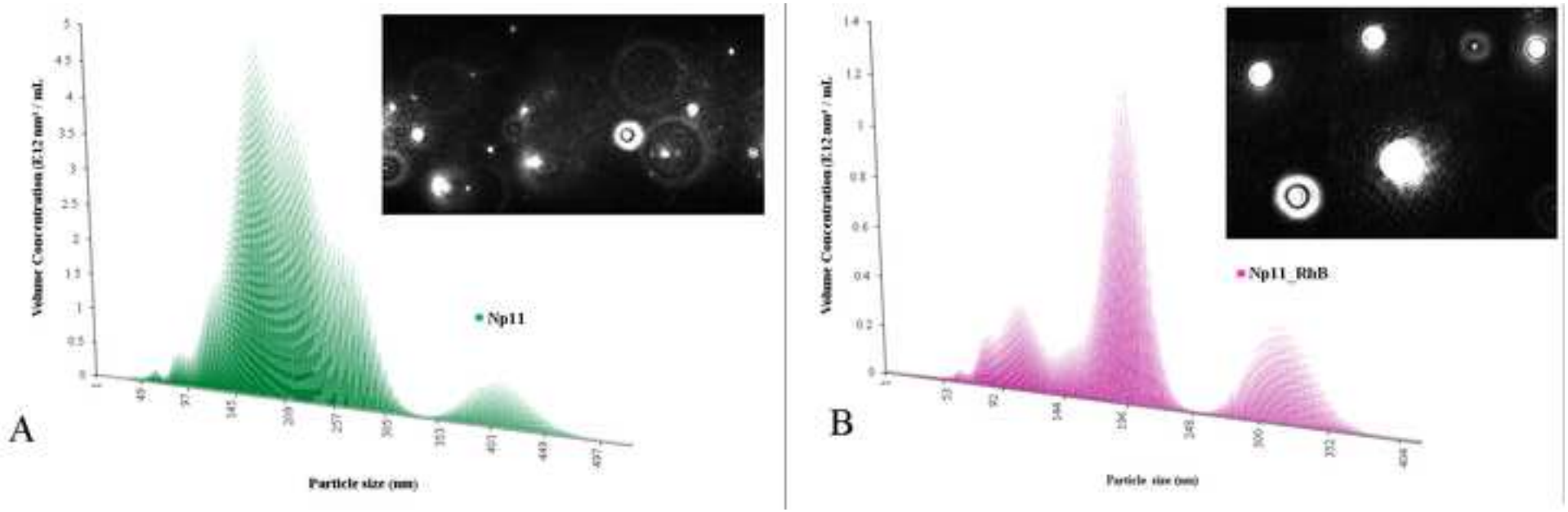

Figure
Click here to download high resolution image

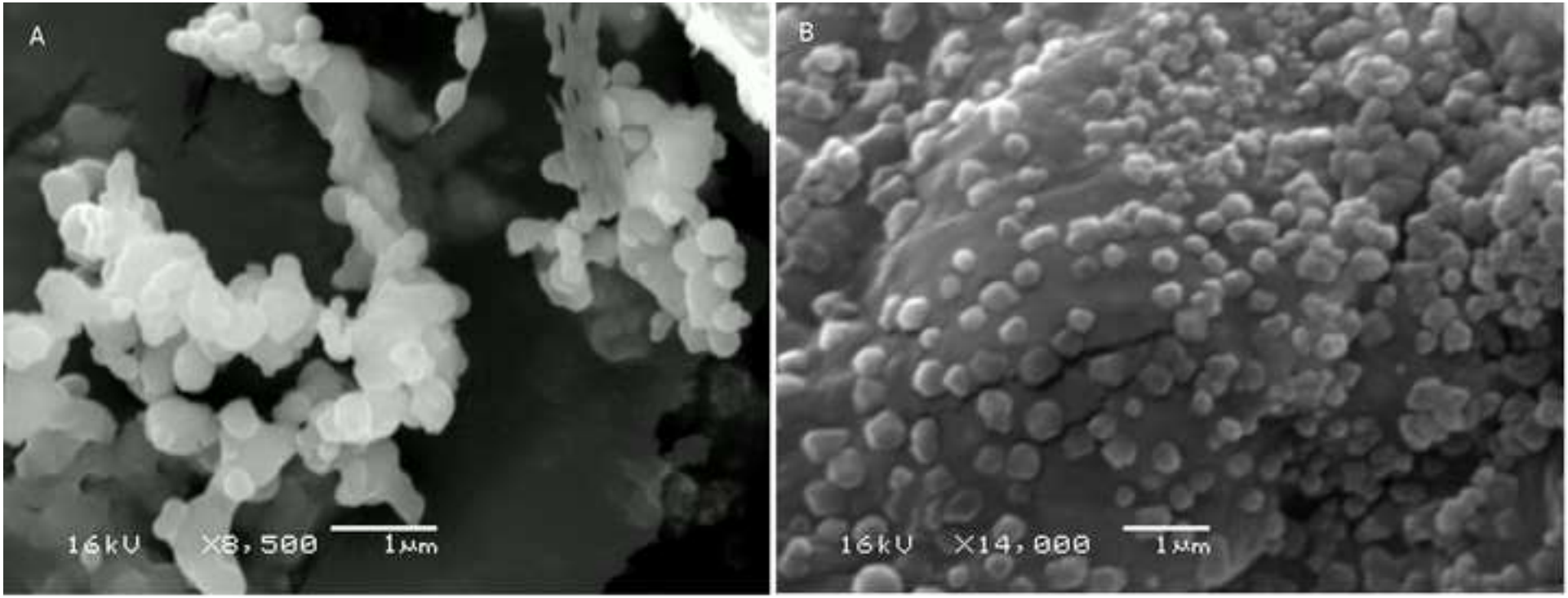

Figure
Click here to download high resolution image

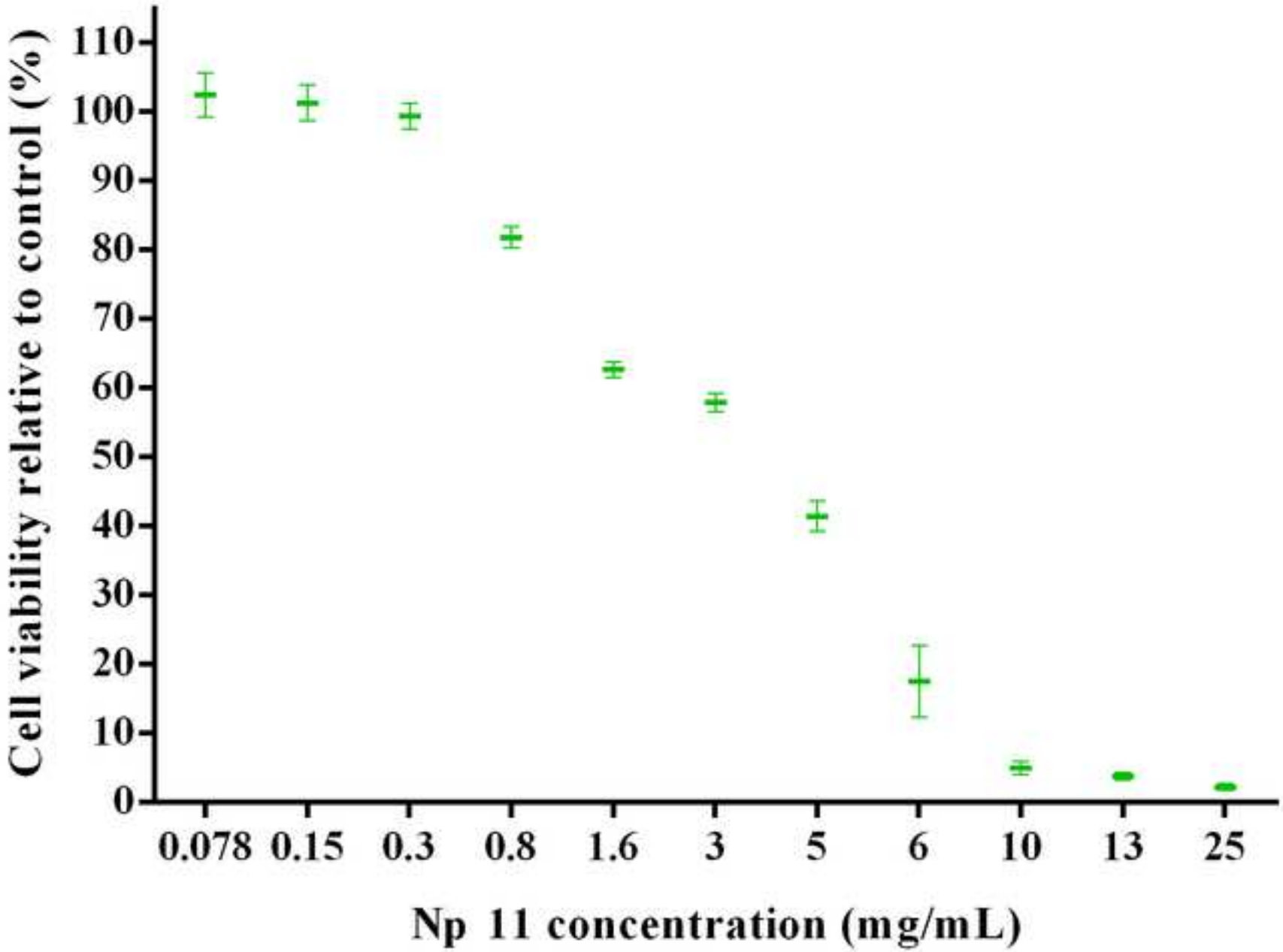

Figure

Click here to download high resolution image

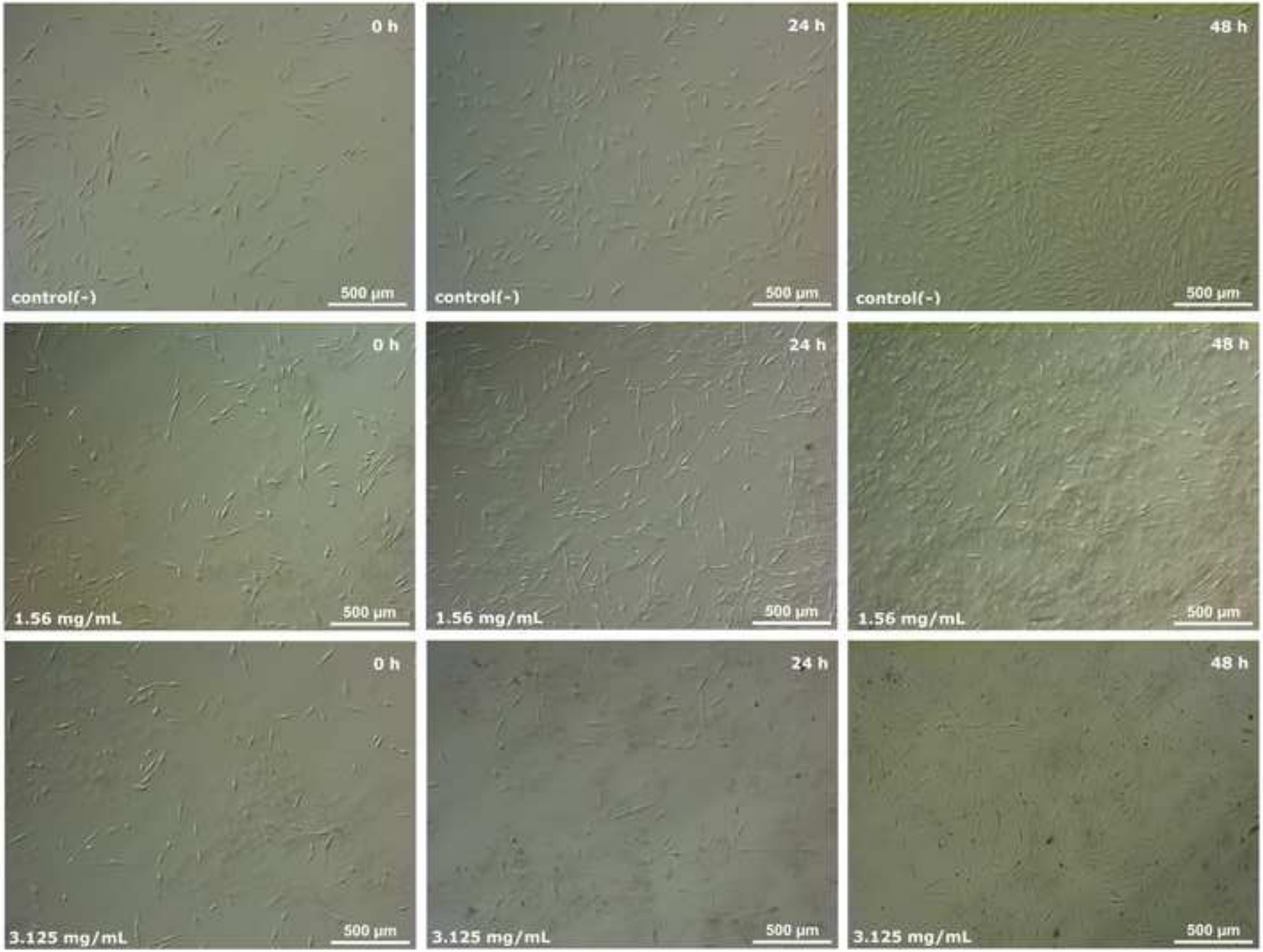

Figure
Click here to download high resolution image

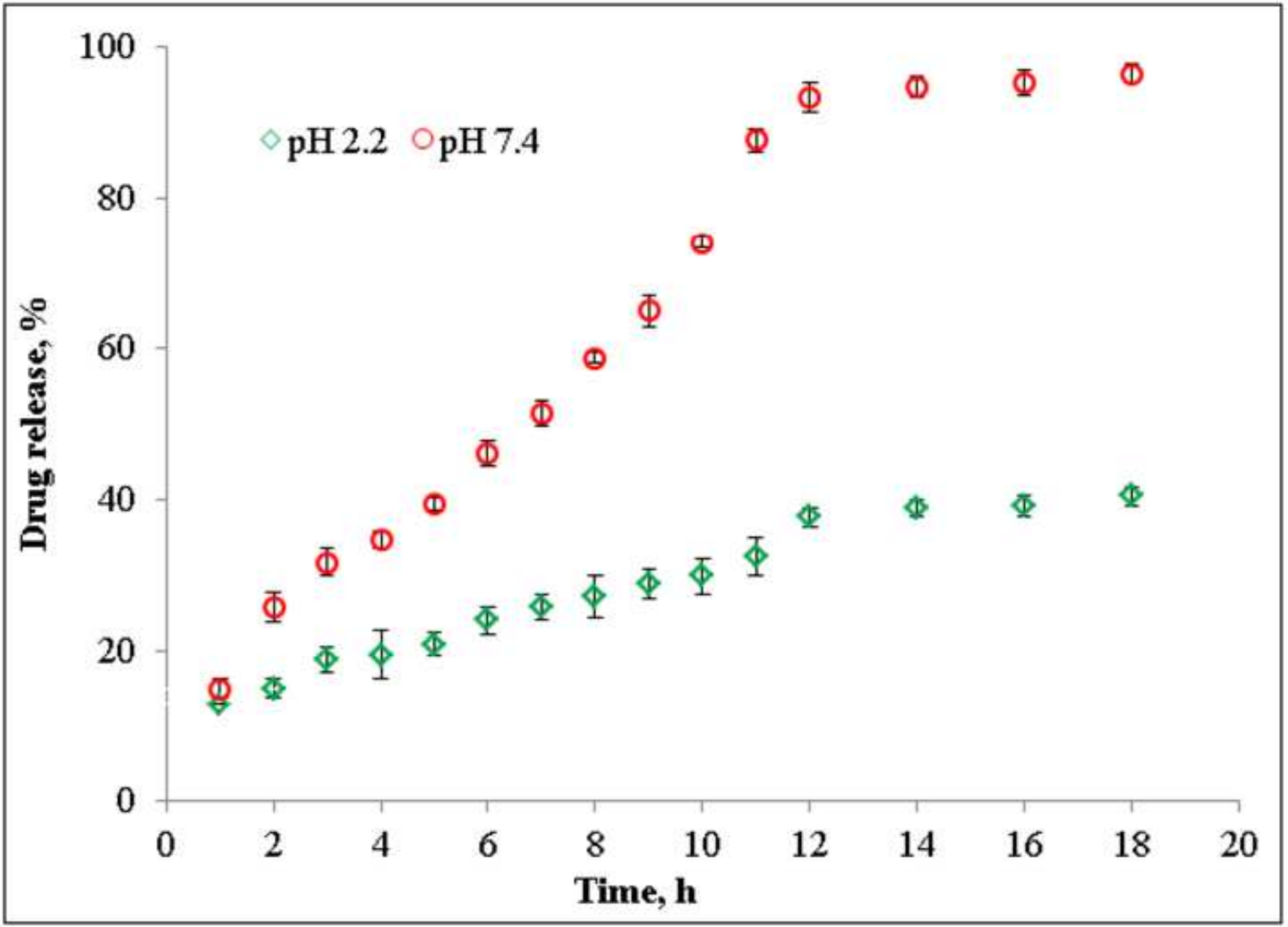

Table

Tables

Table 1. Molecular weight characteristics of GG and CMGG.

Sample	M_w, kDa	PDI
GG	220	1.92
CMGG	261	1.5

Table 2. Characteristics of different nanoparticle formulations prepared.

Batch	CMGG conc., %	STMP conc. %	Size ± SD nm	ζ-potential ±SD, mV	PDI
Np1	0.1	10	780 ± 1.4	-72.6 ± 1.8	0.5
Np2	0.1	5	460 ± 1.3	-39.1 ± 9.5	0.4
Np3	0.1	2.5	360 ± 16.2	-50.6 ± 6.3	0.34
Np4	0.2	5	540 ± 6.6	-39.9 ± 2.5	0.3
Np5	0.2	2.5	594 ± 11.5	-37.5 ± 11.9	0.3
Np6	0.1	1	417.8 ± 1.9	-27.3 ± 9.5	0.2
Np7	0.1	0.5	537.4 ± 8.9	-25.3 ± 4.3	0.3
Np8	0.1	0.25	450.6 ± 12.4	-22.5 ± 8.5	0.31
Np9	0.1	0.2	387.7 ± 0.6	-29.3 ± 2.1	0.25
Np10	0.2	0.2	593.4 ± 1.3	-33.2 ± 1.4	0.12
Np11	0.05	0.2	208.8 ± 0.9	-39.3 ± 1.1	0.11

Table 3. Thermogravimetric analysis

Sample	Step	T_{peak}, ^0C	Weight loss, %	Residue %
GG	I	51.13	8.54	21.73
	II	262.07	69.73	
CMGG	I	51.04	10.70	23.17
	II	241.98	56.57	
	III	478.51	9.56	
Np11	I	70.05	2.34	26.13
	II	492.91	71.53	

Table 4. Entrapment efficiency, size distribution, ζ-potential and PDI for RhB loaded CMGG particles (batch NP11).

NP11, mg	RhB, mg/mL	E_e, %	Size ±SD nm	ζ-potential ±SD mV	PDI
100	5	33.5±0.6	259.5±0.49	-4.8±0.5	0.2
100	1	57.5±0.2	274.3±0.74	-4.57±0.27	0.15
100	0.5	83.2±0.6	318.4±0.8	-13.4±0.57	0.14
100	0.25	61.4±0.4	321±1.22	-9.54±1.37	0.08